

Transport across 48°N in the Atlantic Ocean

RICK LUMPKIN

NOAA/Atlantic Oceanographic and Meteorological Laboratory, Miami, Florida

KEVIN G. SPEER

Department of Oceanography, The Florida State University, Tallahassee, Florida

K. PETER KOLTERMANN

Bundesamt für Seeschifffahrt und Hydrographie, Hamburg, Germany

(Manuscript received 30 May 2006, in final form 27 June 2007)

ABSTRACT

Transports across 48°N in the Atlantic Ocean are estimated from five repeat World Ocean Circulation Experiment (WOCE) hydrographic lines collected in this region in 1993–2000, from time-varying air–sea heat and freshwater fluxes north of 48°N, and from a synthesis of these two data sources using inverse box model methods.

Results from hydrography and air–sea fluxes treated separately are analogous to recently published transport variation studies and demonstrate the sensitivity of the results to either the choice of reference level and reference velocities for thermal wind calculations or the specific flux dataset chosen. In addition, flux-based calculations do not include the effects of subsurface mixing on overturning and transports of specific water masses. The inverse model approach was used to find unknown depth-independent velocities, interior diapycnal fluxes, and adjustments to air–sea fluxes subject to various constraints on the system. Various model choices were made to focus on annually averaged results, as opposed to instantaneous values during the occupation of the hydrographic lines. The results reflect the constraints and choices made in the construction of the model.

The inverse model solutions show only marginal, not significantly different temporal changes in the net overturning cell strength and heat transport across 48°N. These small changes are similar to seasonally or annually averaged numerical model simulations of overturning. Significant variability is found for deep transports and air–sea flux quantities in density layers. Put another way, if one ignores the details of layer exchanges, the model can be constrained to produce the same net overturning for each repeat line; however, constraining individual layers to have the same transport for each line fails.

Diapycnal fluxes are found to be important in the mean but are relatively constant from one repeat line to the next. Mean air–sea fluxes are modified slightly but are still essentially consistent with either the NCEP data or the National Oceanography Centre, Southampton (NOC) Comprehensive Ocean–Atmosphere Data Set (COADS) within error. Modest reductions in air–sea flux uncertainties would give these constraints a much greater impact. Direct transport estimates over broader regions than the western boundary North Atlantic Current are needed to help resolve circulation structure that is important for variability in net overturning.

1. Introduction

The partition of energy and freshwater flux between the ocean and the atmosphere and among various components of the ocean system is a key problem in climate

studies. Bryan (1962) provided the basic decomposition of ocean heat transport into thermal wind, gyre, and Ekman components for a rough estimate of the mean state, especially in the Atlantic Ocean, and many other studies have since contributed to the understanding of this problem. Recent coupled atmosphere–ocean model results suggest that in the northern North Atlantic the interannual variability is dominated by Ekman transports (Shaffrey and Sutton 2004). On longer time

Corresponding author address: Rick Lumpkin, NOAA/AOML/PhOD, 4301 Rickenbacker Causeway, Miami, FL 33149.
E-mail: rick.lumpkin@noaa.gov

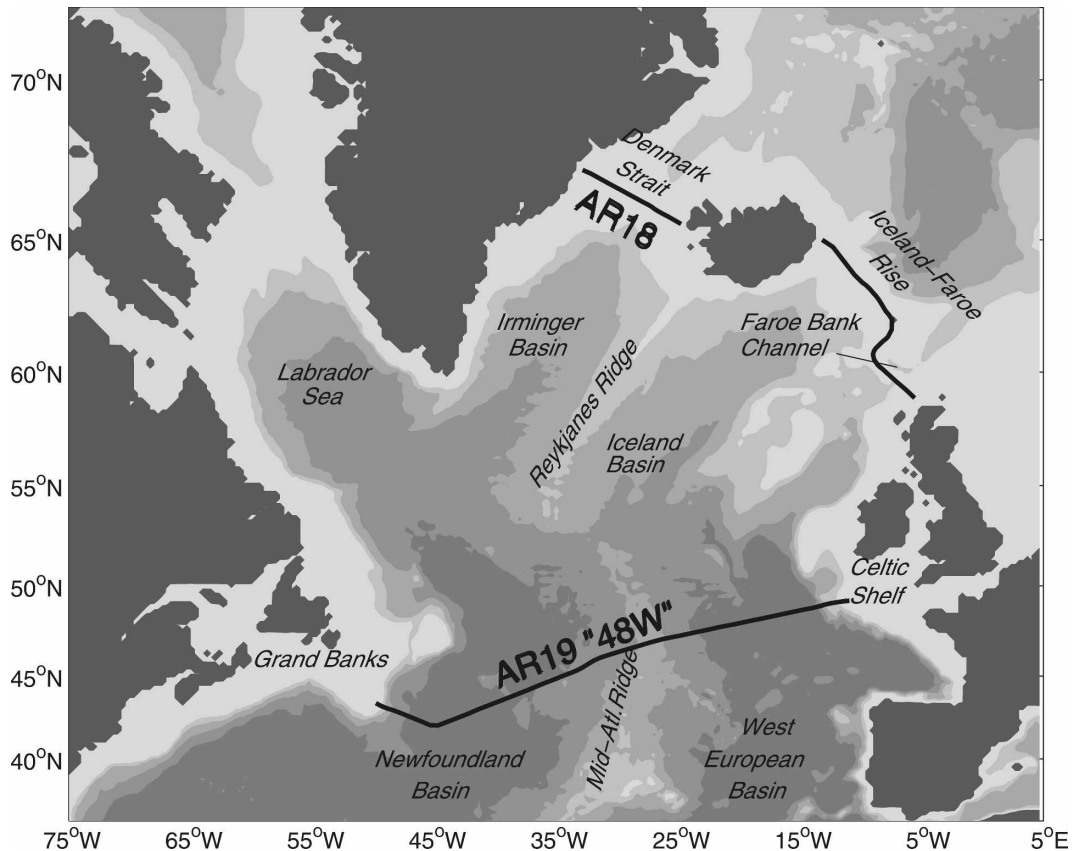


FIG. 1. The North Atlantic Ocean, indicating the locations of geographical features and hydrographic lines mentioned in the text. The five repeats of the 48°N line AR19 used in this study are sufficiently collocated as to be indistinguishable at this scale.

scales the ocean's response to buoyancy forcing appears to dominate overturning (Eden and Jung 2001).

Observational evidence of a long-term decline in overturning has recently been claimed (Bryden et al. 2005), inferred from subtropical trans-Atlantic hydrographic sections and attributed to a reduction in the formation of dense North Atlantic Deep Water (NADW). However, direct current observations of several years' length at the subpolar western boundary do not show any significant long-term changes in this major NADW export route (Schott et al. 2006). On the other hand, direct current measurements are very local and might not reflect larger-scale changes in circulation driven, for example, by shifts in the wind. Many studies point to the central role played by a recurring air-sea interaction pattern, the North Atlantic Oscillation (NAO); a fraction of the observed variability at a wide range of space and time scales is known to be related to this pattern (Häkkinen 1999; Eden and Willebrand 2001; Bersch 2002; Gulev et al. 2003).

The exchange between the subtropical and subpolar gyres across the region near 45°–50°N (Fig. 1) is ex-

pected to be sensitive to climate shifts at higher latitudes and changes in deep convection, and it has been the focus of repeated hydrographic sections over the course of several decades. This latitude band is well suited for measurements of the North Atlantic overturning circulation's strength, because it separates the intense recirculations of the subtropical and subpolar gyres. Koltermann et al. (1999) calculated heat and mass transports near 48°N from hydrographic sections for the years 1957, 1982, and 1993. Their results showed substantial changes, with overturning amplitudes—defined as the maximum in overturning streamfunction, or transport integrated over subthermocline layers—of 10.1, 19.7, and 15.5 Sv ($1 \text{ Sv} \equiv 10^6 \text{ m}^3 \text{ s}^{-1}$) for these respective years. With additional World Ocean Circulation Experiment (WOCE) repeat sections, Lorbacher and Koltermann (2000) extended the time series through 2000 and found that the variations at interannual time scales were as strong, ranging from 13 to 20 Sv, as the apparent lower frequency changes. These variations suggest that the overturning variability range is about 50%, which at an interannual or

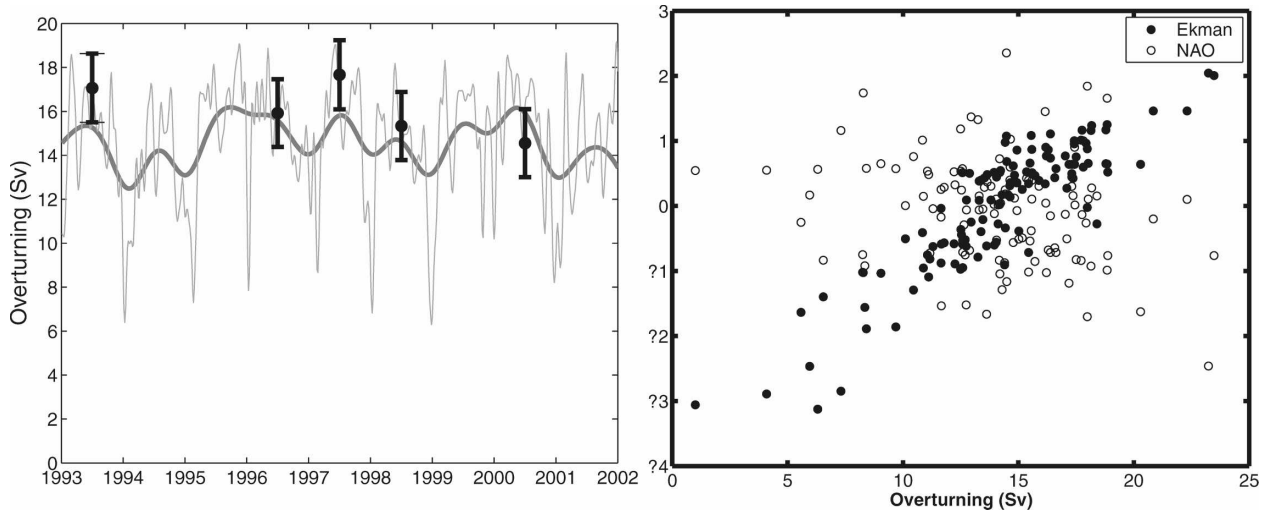


FIG. 2. (left) Overturning [gray lines; smoothed over 11 days (light) and 122 days (dark)] at 48°N from the CLIPPER $\frac{1}{2}^{\circ}$ simulation and independent estimates for the five repeat hydrographic lines (black circles) calculated in this study by inversions with time-invariant mixing. (right) Scatterplot of Ekman transport at 48°N and the NAO index vs meridional overturning from the CLIPPER model. All model quantities are monthly averaged. Ekman transport has been normalized by subtracting a mean value of -3.3 Sv and dividing by the monthly standard deviation of 3.5 Sv. The correlation with overturning is 0.94 ± 0.01 (Ekman) and -0.36 ± 0.07 (NAO).

lower frequency would imply a large heat storage or air–sea flux anomalies in the northern North Atlantic Ocean.

Changes in the North Atlantic overturning have also been estimated from time-varying air–sea flux fields by calculating the net buoyancy transformation of outcropping layers north of a control latitude or section. For example, Marsh (2000) used flux fields created by the National Oceanographic Centre, Southampton (NOC) to calculate changes in the export rates of various North Atlantic Deep Water classes for the period of 1980–90. He found an increasing trend in the export of Labrador Sea Water (LSW) during this period of increasing NAO, compensated for by a decreasing trend in the export of denser classes. As a result of this compensation, no significant decadal trend was found for net overturning strength; interannual variations in overturning strength were stronger, with maxima in 1986 and 1989–90 (Marsh 2000). However, this flux-based approach neglects the impact of mixing on the density structure of the overturning circulation (cf. Speer 1997). Furthermore, air–sea flux fields such as those provided by NOC may contain biases, and the sensitivity of the results to the choice of flux product is unclear when only a single product is used.

Numerical simulation-based studies of overturning variations have generally indicated weak variations at 48°N at interannual time scales. For example, Mauritzen and Häkkinen's (1999) model of the northern North Atlantic, including the polar seas north of the Greenland–Scotland Ridge, showed small interannual

variability in the overturning, on the order of $1\text{--}2$ Sv yr^{-1} , but with a strong seasonal cycle of about 10 Sv at 40°N associated with water-mass volume changes north of that latitude. Mauritzen and Häkkinen (1999) did not attempt to analyze the mechanism of variability but suggested that significant changes in the overturning rate occur only when all three major components vary simultaneously: Labrador Sea convection, Greenland–Norwegian Sea convection, and overflow. Atlantic numerical simulations suggest that the main instantaneous response should be to the net Ekman transport at the latitude of the section (see Eden and Willebrand 2001) with large high-frequency (periods of days) fluctuations but much reduced seasonal and interannual variability of $2\text{--}3$ Sv. Figure 2 shows variations in the North Atlantic overturning from the $\frac{1}{2}^{\circ}$, z -coordinate CLIPPER model run ATL6–26 (A. M. Treguier 2003, personal communication). This run is similar to that described in Treguier et al. (2003), except that ATL6–26 is integrated from rest using daily European Centre for Medium-Range Weather Forecasts (ECMWF) forcing and that some deep anomalies in the earlier run, which are associated with the Romanche Fracture Zone, the Vema Channel, and the Walvis Ridge, have been addressed by adjusting the topography. The CLIPPER model shows pronounced variations of $O(10$ Sv) in the overturning strength at intraseasonal frequencies, primarily associated with wind-driven Ekman transport variations, but the annually averaged overturning is nearly constant at $12\text{--}14$ Sv. These results are in accord with other seasonally or annually averaged Atlantic nu-

merical model simulations of overturning (e.g., Beis-
mann et al. 2002).

In this study, transports across 48°N are estimated from the repeat hydrographic sections, from various air–sea flux climatologies, and from a synthesis of the hydrography and air–sea fluxes using linear inverse box models based on the North Atlantic model of Lumpkin and Speer (2003, hereafter LS03). We also incorporate moored observations of western boundary flow in the North Atlantic. Historical subsurface float data covering the western boundary region and the interior were incorporated in initial calculations, but in the end they were not retained because of inconsistent spatiotemporal coverage and correspondingly ill-defined annual means. Our goal is to combine the information from these data sources to estimate changes in overturning strength and transport in two key water masses—Labrador Sea Water and Lower Deep Water (LDW)—during the period of 1993–2000. We also seek to derive the most accurate observation-based estimate of the time-mean (over this period) circulation at the interface between the subtropical and subpolar North Atlantic.

Our best estimates of transports and their variations come from combining all the information from hydrography, air–sea fluxes, and direct current measurements in the North Atlantic Current using the inverse box model framework. We find variations in the overturning strength (Fig. 2) with a range of just over 3 Sv and a standard deviation of 1.3 Sv. Despite significant variations in the interannual air–sea forcing by heat flux and Ekman transport, neither the observed overturning nor the heat flux shows a significant trend within error. The definition of this error is itself subject to question, because various assumptions are made to make up for missing direct information about the velocity field. At a minimum, the results provide an accurate estimate of the WOCE period mean overturning at 48°N, 16.1 ± 0.7 Sv.

2. Data

a. North America to Europe hydrographic section, 48°N

WOCE line AR19 (A2) ran from the edge of the Grand Banks (at a bottom depth of 65 m) to the Celtic shelf south of Ireland (at a bottom depth of 155 m) nominally along 48°N. The following repeats of this section were carried out under the German WOCE and Climate Variability and Predictability (CLIVAR) programs: AR19a (July 1993), AR19c (May 1996), A2_97 (June 1997), AR19d (May 1998), and AR19f (May 2000; for more information, see Lorbacher and Kolter-

mann 2000). An additional repeat was occupied in October–November 1994, but because of foul weather and time constraints a >300-km gap was unoccupied in the western boundary; we chose not to use the 1994 repeat in this study. The distributions of salinity and neutral surfaces for these sections are depicted in Fig. 3, showing the very high-salinity signature of subtropical-origin water in the western boundary current (the North Atlantic Current), the fresh salinity anomalies characterizing LSW, and the higher salinities in the upper North Atlantic Deep Water layer separating LSW from LDW.

b. Greenland to Scotland and Denmark Strait sections

The role of the exchange with the polar marginal seas and the associated overflow of dense water is a fundamental element of the Atlantic deep circulation. For the inverse box models, we include hydrographic sections across these sills (Fig. 1): WOCE line AR18 (Denmark Strait, Chief Scientist S.-A. Malmberg, conducted September 1995) and a composite Iceland–Scotland line. Hydrographic observations for the composite line were chosen to run along the crest of the Iceland–Faroe Rise from Iceland to the Faroe Shelf, and then southwest across the Faroe Bank Channel to the Faroe Bank, then southeast along the Wyville–Thompson Ridge to the Hebridean shelf off the Scottish coast. Three segments from the 1986–88 North Atlantic and Norwegian Sea Exchange (NANSEN) experiment span most of this range, terminating on the Iceland–Faroe Rise (leaving a 230-km gap between Iceland and this composite section). This gap was filled by a set of observations collected in June 1998 as part of the Variability of Exchanges in the Northern Seas (VEINS) experiment. Despite the 10-yr separation between the NANSEN and VEINS observations, the sections did not exhibit a discontinuity in hydrographic properties (LS03).

Any variability of overflow would in turn generate variability in deep water overturning in the subpolar region directly and through entrainment. However, while a freshening trend in Nordic Sea water has been observed over the past four decades (Dickson et al. 2002), the observed magnitude should—according to a range of numerical experiments—be associated with a decrease in the Atlantic overturning strength of only ~ 1 Sv (Latif et al. 2006). Direct observations of the overflow intensity (Girton et al. 2001) suggest that the variability at periods greater than a few days is a small fraction of the overflow, although a recent study by Macrander et al. (2005) has suggested that the Denmark Strait’s annually averaged overflow has decreased from 3.7 in 1999 to 3.1 Sv in 2003. Changes of $O(1)$ Sv

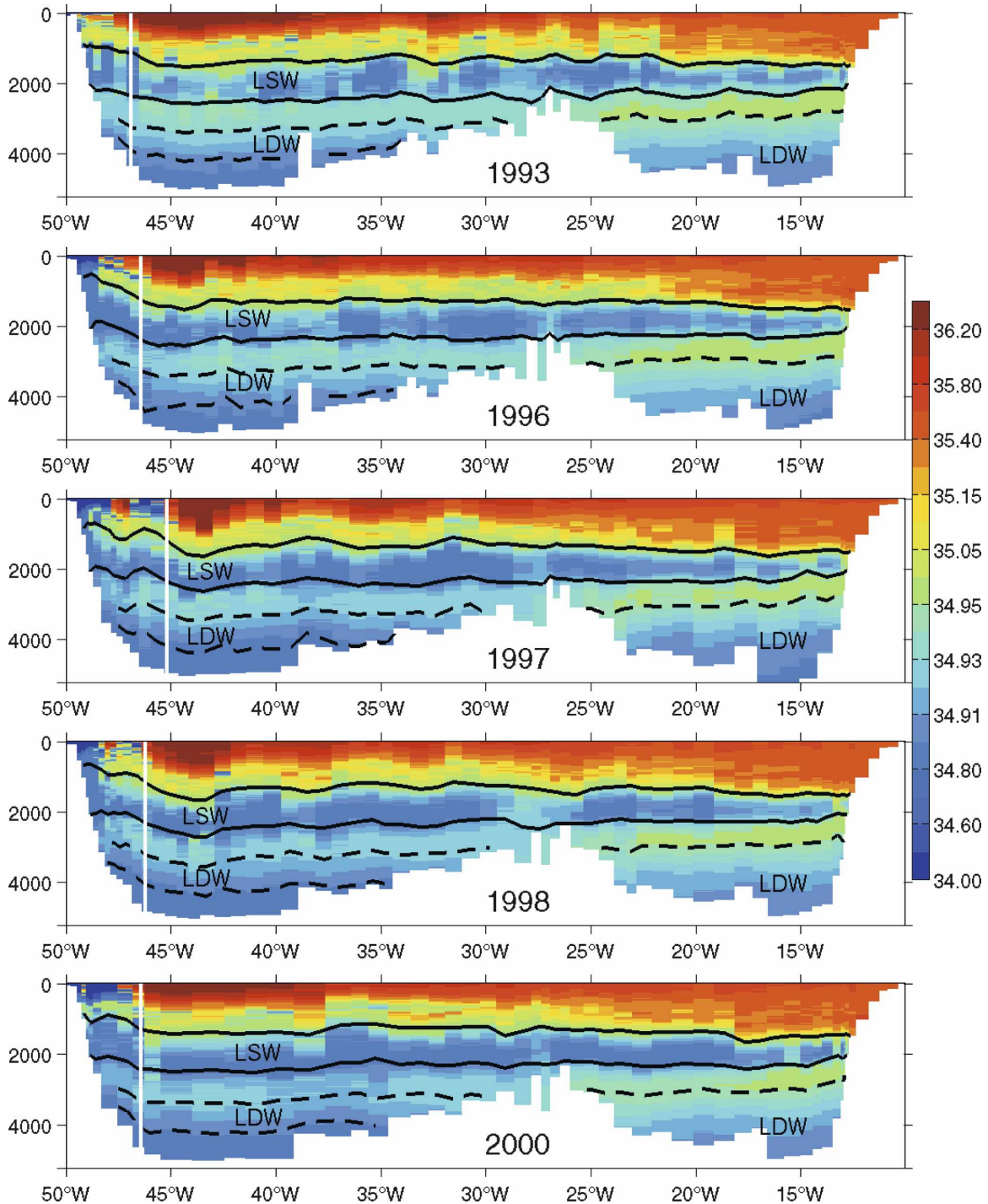


FIG. 3. Salinity at 48°N from hydrographic repeats. Vertical axes are pressure (dbar). Solid black lines indicate interfaces $\gamma'' = 27.88$ and 27.98 , which bound LSW. The upper value was used as the level of no motion for thermal wind transport calculations. Dashed black lines indicate interfaces $\gamma'' = 28.06$ and 28.12 , which delineate LDW. Vertical white lines indicate the core of the NAC, determined from the isotherm $\theta = 10^\circ\text{C}$.

are small enough to be absorbed by model error in the solutions presented here. Larger changes in our results are due to density-changing processes within the sub-polar North Atlantic.

c. Air-sea fluxes

Estimates of air-sea fluxes of heat, freshwater, and wind stress were taken from two sources: the National

Centers for Environmental Prediction–National Center for Atmospheric Research (NCEP–NCAR) reanalysis, version 2 (Kalnay et al. 1996), and the NOC reanalysis of the Comprehensive Ocean–Atmosphere Data Set [COADS; previously Southampton Oceanography Center (SOC)]. We used the following two versions of the NOC COADS: one (Grist and Josey 2003) was adjusted to satisfy time-mean constraints on global heat input and on heat transport across key latitudes, and the other (Josey et al. 1998) was not adjusted to meet these constraints (“unadjusted NOC COADS”). The unadjusted product has a global ocean gain of 30 W m^{-2} , while the adjusted product has a global ocean loss of -5 W m^{-2} (Grist and Josey 2003). Grist and Josey did not impose a heat transport constraint at 48°N in the Atlantic, although they required a time-mean northward transport of $1.22 \pm 0.30 \text{ PW}$ across 24°N (Hall and Bryden 1982) and $0.28 \pm 0.06 \text{ PW}$ across $\sim 56^\circ\text{N}$ (Bacon 1997) in the Atlantic.

Wind stress was used to calculate Ekman transport. Transport of heat and salt was calculated by applying the Ekman transport to the 10-m climatological monthly values from Levitus and Boyer (1994) and Levitus et al. (1994); an annual net transport was given by the sum of the 12 monthly transports multiplied by the monthly tracer values.

3. Transports calculated separately from hydrography and air–sea fluxes

Previous observation-based investigations have calculated transports across 48°N using either hydrography (Koltermann et al. 1999; Lorbacher and Koltermann 2000) or air–sea fluxes (Marsh 2000). Before proceeding to synthesize these data using the inverse box model framework, we make analogous calculations to these previous studies to determine the impact of reference-level velocities and different air–sea flux products. We explicitly compare these independently calculated transports before combining them in a framework that adjusts both the reference velocities and the air–sea fluxes.

a. Transports from hydrography

Transports based on hydrography alone do not incorporate property conservation in density layers or water-mass formation rates based on air–sea fluxes, but they are a direct function of baroclinic changes in the hydrography. The transports depend on reference-level choices that can be derived from, for example, current meter observations. In the inverse model framework (section 4), these choices are used as the initial conditions for the inversions.

For all 48°N repeat sections, transports were calcu-

lated using thermal wind integrated from a level of no motion on a constant neutral density γ^n (Jackett and McDougall 1997) interface, $\gamma^n = 27.88$ ($\sigma_\theta \approx 27.74$), with a mean depth of 1275 m (see Fig. 3). For each repeat, a uniform offset of $0.43\text{--}1.02 \text{ mm s}^{-1}$ was added as needed to achieve a net northward mass transport of 2.46 Sv, balancing the time-mean southward Ekman transport. Net transports of heat, Labrador Sea Water ($27.88 \leq \gamma^n \leq 27.98$), and dense Lower Deep Water ($28.06 \leq \gamma^n \leq 28.12$) are shown in Fig. 4 and their values are given in Table 1. Also shown is the overturning strength, defined as the maximum in the bottom-to-top streamfunction in density coordinates. The assumption of a middepth zero reference-level velocity reduces the influence of lateral variations of flow with large vertical scale but tends to increase the overturning component. The result shows an overturning cell of $19 \pm 3 \text{ Sv}$, with no significant trend.

Without additional modifications, the level-of-no-motion choice described above produces net top-to-bottom western boundary transports of 40–50 Sv. In contrast, observations with bottom pressure gauges, deep current meters, and inverted echo sounders (IESs) in 1993–95 indicate that the mean transport in the western boundary reaches a maximum of over 100 Sv (Meinen 2001). To include motion on the thermal wind reference level, Koltermann et al. (1999) and Lorbacher and Koltermann (2000) assumed that the depth-averaged transport was equal to the Sverdrup transport. However, the validity of this assumption has been questioned (cf. Bryden and Imawaki 2001) because Sverdrup transports are far weaker than the observed transport.

Unfortunately, no direct current measurements of the North Atlantic Current (NAC) were collected over the period of 1993–2000. The NAC mooring array (Meinen and Watts 2000) ran along the western boundary segment of the AR19 sections (WOCE current meter line ACM6) from $44^\circ 35'$ to $48^\circ 38' \text{W}$ during the period of August 1993–February 1995. It is possible, in principle, to define reference velocities from these observations in geographical coordinates. However, as noted by Meinen (2001), the NAC and Mann Eddy system migrate over ~ 100 nautical miles; this can be seen in the 48°N repeats (Fig. 3), which supports using a coordinate system referenced to the NAC for defining absolute velocities for individual hydrographic lines. The best choice for such a system is the stream coordinate system, in which the NAC core and origin of the system are defined as the longitude where the 10°C isotherm crosses 450 dbar (Meinen 2001). The western edge of the NAC is about 200 km west of the core in this stream coordinate system. From the NAC mooring

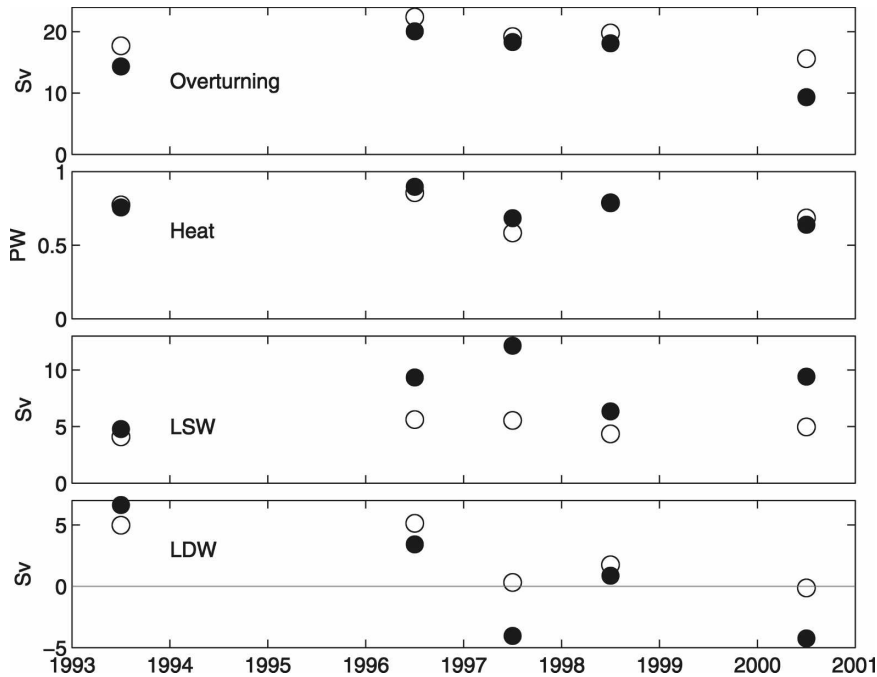


FIG. 4. (from top to bottom) Overturning and transports of heat (positive northward), LSW (positive southward), and LDW (positive southward) across 48°N calculated from hydrography, using a level of no motion (open circles) and including nonzero reference velocities (black bullets). Heat transports do not include the Ekman component.

observations, we calculated the time-mean profile of velocity on the thermal wind reference level $\gamma^n = 27.88$ in the stream coordinate system. The resulting velocities (Fig. 5) are northward in the NAC and southward (-6.8 cm s^{-1}) against the shelf break [and over the deep western boundary current (DWBC)]. These velocities increase the net northward transport to approximately 115 Sv (Meinen and Watts 2000), with 145 Sv northward and 30 Sv southward, between -200 and $+200$ km in stream coordinates.

To obtain hydrography-based transport calculations including this nonzero flow at the reference level, we added the reference-level velocity profile $v(d)$, where d is the stream coordinate distance, to the thermal wind field from $d = -200$ to 0 km. The stream profile from 0 to $+200$ km was stretched or compressed to span the time-dependent distance between the NAC core (identified as described above) and the center of the Mann Eddy (Mann 1967) in the hydrographic repeat line, identified by a peak northward cumulative west-east transport. West of -200 km (i.e., in the Labrador Current) up to the shelf break (at a bottom depth of 500 m), $v(d)$ was assumed to be -6.8 cm s^{-1} (negative southward), the westernmost observed value. For shallow casts west of the shelf break, a bottom zero-velocity reference was used. Bottom triangles were found to

have a small influence on net transports in the western region. For each repeat, the profile of $v(d)$ from -200 km to the Mann Eddy center was multiplied by a constant coefficient so that the net transport was 115 Sv, matching the time-mean value from the mooring array. (The inverse models, described below, are free to adjust this profile to accommodate year-to-year variations in both net and layer transports.)

Excluding the North Atlantic Current western boundary region, thermal wind referenced to $\gamma^n = 27.88$ yields a negligible net transport (0–5 Sv). This does not

TABLE 1. Transports across the 48°N sections calculated from thermal wind: net overturning, LSW and LDW export (positive southward), and heat (positive northward). The first value in each cell is from the level-of-no-motion calculation; numbers in parentheses are from the calculations with nonzero reference-level velocities.

Year	Overturning (Sv)	LSW (Sv)	LDW (Sv)	Heat (PW)
1993	17.7 (14.3)	4.1 (4.8)	5.0 (6.6)	0.77 (0.76)
1996	22.4 (20.1)	5.6 (9.3)	5.1 (3.4)	0.86 (0.90)
1997	19.2 (18.3)	5.5 (12.1)	0.3 (−4.1)	0.58 (0.68)
1998	19.8 (18.1)	4.3 (6.3)	1.8 (0.9)	0.79 (0.79)
2000	15.6 (9.3)	5.0 (9.4)	−0.1 (−4.3)	0.68 (0.64)
Mean	18.9 (16.0)	4.9 (8.4)	2.4 (0.5)	0.74 (0.75)

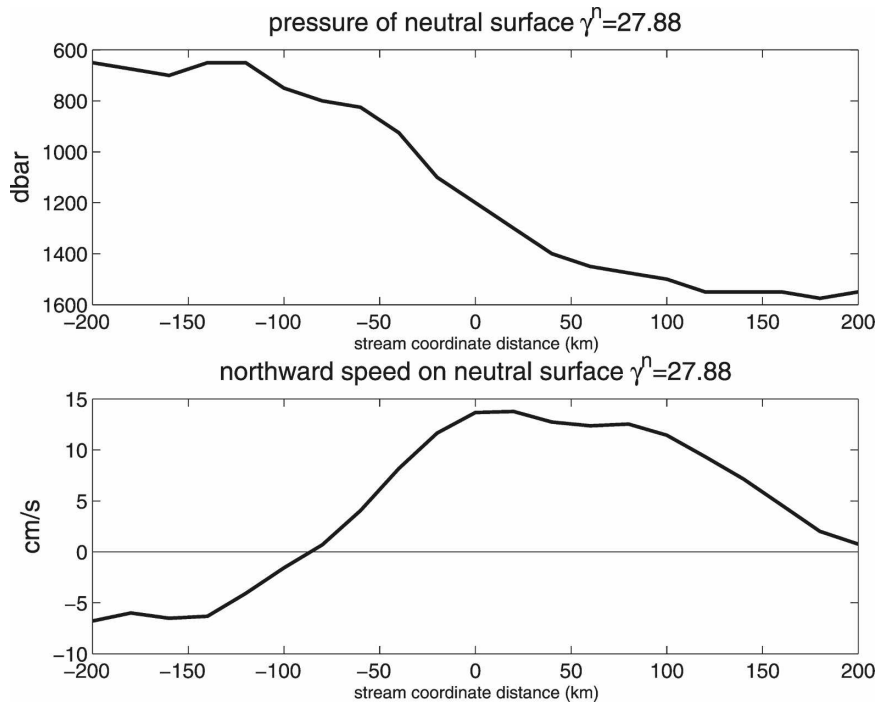


FIG. 5. (top) Time-mean pressure of the thermal wind reference level $\gamma^n = 27.88$ in stream coordinates, calculated from the NAC array (Meinen and Watts 2000; Meinen 2001). (bottom) Northward speed (negative southward) on the reference level.

balance the 115 Sv northward flow in the western boundary current, so reference-level velocities east of $\sim 45^\circ\text{W}$ must act to recirculate water southward.

Immediately offshore of the North Atlantic Current, the primary recirculation may be identified with the semipermanent anticyclonic Mann Eddy, which has a swirl transport estimated at 50–60 Sv (Reiniger and Clarke 1975; Meinen 2001). The western side of this eddy is often indistinguishably joined with the western boundary flow and is included in the 115 Sv net transport discussed above. The eastern side may be identified from the upward-sloping isopycnals east of 45°W in the sections. Thermal wind with a middepth reference level at $\gamma^n = 27.88$ produces a net southward transport in the eastern Mann Eddy of only 10–30 Sv in the various sections. A deeper reference level produces greater southward recirculation, but in any case we adjust the initial field to agree with the more directly inferred transports from Reiniger and Clarke (1975); thus, moving reference levels has little net effect. For each section, we added southward speeds to the thermal wind profiles within the eastern Mann Eddy to increase the net southward transport to 55 Sv (Meinen 2001). The southward speeds ranged from 2.5 to 6.3 cm s^{-1} . In contrast to Schott et al. (2004), we infer that the Mann Eddy recirculation is a significant part of the western

boundary current regime. This flow cannot be neglected when calculating net transports across 48°N .¹ Direct current meter measurements have yet to resolve this element of the circulation.

Finally, a uniform (for each repeat) southward reference speed was added to all remaining pairs east of the Mann Eddy to bring the overall geostrophic transport to 2.5 Sv northward, balancing the mean southward Ekman transport across the section. A uniform southward speed (as opposed to a more structured velocity field) was judged to be “best” because it was the simplest choice in the absence of time-varying absolute velocity measurements in the eastern North Atlantic basin. This southward reference-level speed varied from 6 to 9 mm s^{-1} for the various 48°N repeats.

After making these adjustments to a level of no motion at $\gamma^n = 27.88$, the net transports across 48°N in different layers are shown in Fig. 4, with values given in Table 1. The largest changes in layer transports caused by adding nonzero reference-level velocities are

¹ Some support for a strong recirculation is evident in an analysis of surface pressure from surface drifters, satellite data, and geostrophic model constraints (Niiler et al. 2003). Our own analysis of subsurface float data also suggests strong recirculation but does not provide a useful quantitative constraint.

found in the Labrador Sea Water layers. In the level-of-no-motion calculations, nearly all of the roughly 5 Sv of net southward transport was in the Deep Western Boundary Current; interior flow to the east was negligible. With the adjusted reference velocities, the net southward transport of LSW is larger by about 50%. The new set of transports has a much stronger 10–15-Sv southward transport of LSW. A larger amount, 20–25 Sv, flows north within the NAC and western part of the Mann Eddy. In the immediate recirculation of the eastern side of the Mann Eddy, about 10 Sv of LSW is carried southward. Thus, the net transport of LSW across the western boundary current system (including the Mann Eddy) is nearly zero (less than 5 Sv northward), with the adjusted reference-level velocities based on moored observations. East of the Mann Eddy and distributed across the interior of the sections, LSW flows southward to yield a cumulative net of 5–12 Sv.

b. Transports from air–sea fluxes

Buoyancy-driven transformation across outcropping isotherms (Walín 1982) or isopycnals can be calculated from monthly values of air–sea heat and freshwater fluxes (cf. Large and Nurser 2001). In practice, this is done for a set of fluxes by calculating the density of surface water from sea surface temperature (provided by the flux product) and sea surface salinity [usually from a monthly climatology; Levitus and Boyer (1994) and Levitus et al. (1994) used here], calculating the buoyancy transformation for each grid of the product driven by the fluxes and integrating the (typically monthly) results in density bins for the region of interest (cf. LS03, their appendix C, sections a–c). The convergence of this mass transfer in a particular density range gives the formation rate of water with this density. Marsh (2000) used this approach to calculate the export of North Atlantic Mode Waters for the period of 1980–93 from unadjusted NOC COADS. In this section we repeat these calculations for the subpolar North Atlantic, between the 48°N section and the Greenland–Scotland Ridge, using the unadjusted and adjusted NOC COADS products and the NCEP–NCAR reanalysis version 2 product.

The mean transformation over the period of 1981–97 (not shown) is qualitatively similar for the three products, with a peak of 10.0 (NOC unadjusted), 11.8 (NCEP), and 13.2 Sv (NOC adjusted) at $\gamma^{\prime} = 27.4$ – 27.5 ($\sigma_{\theta} = 27.3$ – 27.4). Changes in net dense-water formation and in LSW formation from unadjusted or adjusted NOC COADS are qualitatively consistent with the results of Marsh (2000). Over the period of 1990–97, the

rate of LSW formation has decreased (Fig. 6), reversing the increasing trend of 1980–90 (Marsh 2000). Overturning, in contrast, has remained relatively constant at decadal scales after peaks in 1986 and 1989–90 (Marsh 2000). Our overturning values (Table 2) are smaller than Marsh's because of the smaller region in which we integrated the air–sea fluxes; his values include transformation associated with Subtropical Mode Water formation south of 48°N. They are also smaller than the net overturning across 48°N from thermal wind calculations (Fig. 4), primarily because air–sea transformation north of the Iceland–Scotland sections has been neglected. When transformation in the Norwegian Sea is included, the year-to-year variability in net dense-water formation is similar to that shown in Fig. 6 (with a correlation coefficient of 0.83), but with the mean increased by 6.5 Sv. According to the inverse model solutions presented below, the majority of this transformation ($5.3 \text{ Sv} \pm 0.4 \text{ Sv}$) is partitioned into the dense overflows at a neutral density greater than 28.0. Thus, additional dense water is returned to the North Atlantic through the Denmark Strait and Faroe Banks Channels, and it is represented in the inverse model solutions by overturning across AR18 and the Iceland–Scotland sections (Fig. 1).

When transformation and formation rates are calculated from the NCEP fields, multiyear trends resembling the NOC COADS results are obtained (Fig. 6). Year-to-year variations in the net formation of dense water (corresponding to maximum transformation) from adjusted NOC and NCEP data are similar, with a 1981–97 correlation of 0.66 (97% confidence level). In contrast, LSW formation rates from the two products are uncorrelated. On an annual basis, the NOC-derived LSW formation rate is weakly but significantly correlated (correlation coefficient 0.62, 99% confidence) with the NAO Lisbon–Iceland index (Hurrell 1995). The NCEP-derived formation rate is uncorrelated with the NAO. These discrepancies indicate that the formation and export of Labrador Sea Water are sensitive to the flux product used. Until flux uncertainties can be reduced, information from hydrography and current measurements are also needed to determine Labrador Sea Water transports.

4. Inverse box model

The inverse box model formalism allows information from hydrography, direct current measurements, and air–sea fluxes to be synthesized in a framework that provides formal error bars on the resulting transports. Here we perform five inversions, one for each repeat of the 48°N line, using that line and the time-invariant lines along the Greenland–Scotland Ridge to define a

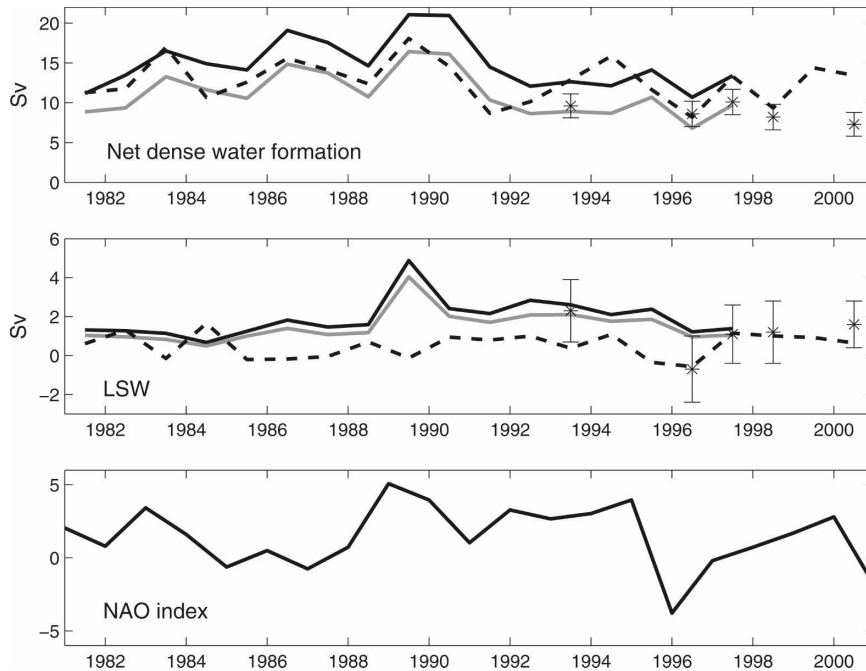


FIG. 6. Formation (Sv) driven by air–sea fluxes from adjusted NOC COADS (solid black), unadjusted NOC COADS (solid gray), and NCEP–NCAR reanalysis version 2 (dashed black) in the subpolar North Atlantic (see Fig. 1), 1981–2000. Yearly averages have been calculated from monthly values from July of the previous year through June of that year. (top) Total dense-water formation (peak value of air–sea transformation); asterisks with error bars show inverse model results: overturning across 48°N minus mean overturning (6.5 Sv) across the Greenland–Scotland sections. (middle) LSW formation by air–sea fluxes (convergence of buoyancy transformation in the range of $27.88 \leq \gamma'' \leq 27.98$); asterisks with error bars show inverse model results: net export of LSW across 48°N minus the mean formation of LSW from subpolar interior mixing (5 Sv). (bottom) Winter NAO index (Hurrell 1995).

subpolar North Atlantic box (Fig. 1). The inverse model is a least squares adjustment from an initial state to meet imposed integral constraints: mass and property conservation north of 48°N . The initial states vary from section to section because of changes in the hydrographic structure and imposed reference velocities as well as changes in the air–sea fluxes (as described in the previous section). We use the nonzero reference-level velocities described in section 3 to have the best

possible initial state with respect to the DWBC, NAC, and net transports. These nonzero reference-level velocities are freely adjusted by the inversions; for example, the time-mean transport values described above are not imposed as a constraint on the inverse model solutions. Instead, the model is free to adjust these transports to accommodate the integral conservation constraints and the temporal changes in air–sea forcing and hydrographic structure at 48°N .

TABLE 2. Yearly averaged values of net dense-water formation, LSW formation, subpolar heat loss, and subpolar freshwater gain calculated from adjusted NOC (aNOC), unadjusted NOC (uNOC), and NCEP–NCAR reanalysis (NCEP) fields, for the years of AR19 repeats.

Year	Net dense (Sv)			LSW (Sv)			Heat (PW)			Freshwater ($10^3\text{ m}^3\text{ s}^{-1}$)		
	aNOC	uNOC	NCEP	aNOC	uNOC	NCEP	aNOC	uNOC	NCEP	aNOC	uNOC	NCEP
1993	12.6	8.9	12.9	2.6	2.1	0.4	0.42	0.25	0.26	96	96	58
1996	10.7	6.8	8.2	1.2	1.0	−0.6	0.27	0.11	0.14	101	101	73
1997	13.4	9.7	13.3	1.4	1.1	1.1	0.38	0.21	0.26	74	74	69
1998	—	—	9.3	—	—	1.0	—	—	0.15	—	—	85
2000	—	—	13.4	—	—	0.6	—	—	0.22	—	—	75

a. Model configuration

Complete information about model implementation can be found in LS03. A summary is provided here, with more details found in the appendix for the reader's convenience. In summary, the model seeks solutions that conserve mass, salt anomaly $\rho(S - 35)/1000$, and potential temperature in 45 neutral-density (Jackett and McDougall 1997) layers. Net silica is also conserved within the box to within $\pm 500 \text{ kmol s}^{-1}$ (Robbins and Toole 1997).² Mass in each layer is conserved following the formation equation $(d/dt)\Delta V = -\delta\rho\partial_\rho(\Psi + F_\rho - \partial_\rho D_\rho)$. This equation combines volume and buoyancy conservation, and it explicitly separates diapycnal transformation into its surface (air–sea flux driven) and subsurface (interior mixing) components. Here, ΔV is the layer volume, and Ψ is the overturning streamfunction from the zonally integrated velocity in each layer; the air–sea formation rate F_ρ is calculated from the monthly air–sea buoyancy fluxes for the 12-month period predating the section as described in section 3; and $\partial_\rho D_\rho$ is the diapycnal flux of buoyancy caused by subsurface mixing.

The model solves three types of unknowns: v_{ref} , the thermal wind reference velocities, one for each station pair in the hydrographic sections; $\partial_\rho D$, the property-dependent diapycnal flux between each of the 45 layers; and F^* , adjustments to the air–sea heat and freshwater fluxes and wind stress on each of the 45 layers. Solutions satisfying the imposed constraints were found via a Gauss–Markov estimation (Wunsch 1996). Some experimental solutions were found by inverting all repeat sections at once, which had the potential advantage of connecting the mass budgets across time with an additional constraint requiring that mass storage cannot be arbitrarily large. However, because these solutions were not significantly different, the results shown here were those obtained by inverting each realization (five in all) independently.

Each of the unknowns has a prior variance and, in principle, a covariance associated with it, to which the model needs to be able to make local adjustments to fluxes and to satisfy constraints. These were chosen following simple principles and established values where possible from field experiments (see the appendix). A guiding principle is to adopt error bounds and con-

straints that tend to minimize diapycnal fluxes across those isopycnals that do not outcrop within a box (LS03). Model imbalances are estimated as well, but because the only dynamics are thermal wind, Ekman transport and surface heat, and freshwater flux–driven transformation, these are not interpreted here dynamically but rather as mass storage. These errors are not constrained in time, for example, from one repeat section to the next; however, accumulated residual rms storage is equivalent to an error of only 1 Sv or less in each layer.

As in LS03, differences between the buoyancy transformation and air–sea input of heat and freshwater using NCEP data and NOC COADS (unadjusted and adjusted) were used as estimates of the error bars on these fluxes. These error estimates were used to set the allowed range of adjustment for air–sea fluxes and associated transformation in the inversions. Because the NOC COADS product terminates after December 1997, mean differences between the two products for the 1993, 1996, and 1997 inversions were used to estimate the errors on the NCEP-derived curves for the 1998 and 2000 inversions. Adjusted NOC COADS oceanic heat losses were consistently larger than those from NCEP for the pre-1998 inversions; the mean of the two products was used as the preinversion air–sea flux curve. For the 1998 and 2000 inversions, the preinversion fluxes were reduced from the NCEP-derived integrated fluxes by the mean offset of the pre-1998 values. The inverse model adjusts the air–sea fluxes according to the constraints of the full set of data.

An important issue when repeat sections are used is the choice of averaging interval. In this analysis, subpolar transformation was calculated from air–sea fluxes during the 12 months preceding the occupation of a repeat line. This choice is subjective. A shorter averaging period leads to large imbalances because of the seasonal cycle; a longer averaging period dampens the effect of interannual air–sea forcing variability. In principle, one would want to integrate the flux fields over a time scale comparable to that for anomalies to propagate from source regions in the Labrador and Irminger Seas to the 48°N hydrographic line. A recent study of repeat hydrography in the subpolar North Atlantic (Stramma et al. 2004) indicates that this time scale is 1–2 yr in the deep western boundary current. Longer integration times might be more appropriate for interior deep currents, while shorter ones would apply to near-surface currents.

b. Inverse model solutions

First, we address a fundamental question: Do the observations provide any significant evidence for change?

² Robbins and Toole (1997) used 100 kmol s^{-1} ; a larger value was chosen here to be more conservative regarding potential riverine input. Final silicate transports were $24\text{--}27 \text{ kmol s}^{-1}$ southward across the northern sections in the various inversions. The net southward transports across 48°N in the fixed mixing inversions were 47 ± 70 (1993), 48 ± 74 (1996), 34 ± 77 (1997), 98 ± 61 (1998), and $20 \pm 71 \text{ kmol s}^{-1}$ (2000).

TABLE 3. Transports across the 48°N sections from the inverse model solutions: net overturning, LSW and LDW export (positive southward), and heat (positive northward). The first value in each cell is from the inversions with time-varying mixing; numbers in parentheses are from the inversions with time-invariant mixing. Standard error bars on the mean values assume that the standard errors for each repeat are independent.

Year	Overturning (Sv)	LSW (Sv)	LDW (Sv)	Heat (PW)
1993	15.1 ± 1.9 (17.1 ± 1.6)	5.6 ± 1.8 (7.3 ± 1.3)	1.6 ± 3.1 (0.4 ± 1.7)	0.55 ± 0.08 (0.59 ± 0.07)
1996	17.8 ± 2.2 (15.9 ± 1.5)	7.4 ± 1.9 (6.3 ± 1.3)	1.6 ± 3.2 (0.7 ± 1.8)	0.51 ± 0.08 (0.47 ± 0.07)
1997	18.9 ± 2.1 (17.7 ± 1.6)	9.2 ± 2.1 (7.8 ± 1.2)	-1.8 ± 3.7 (-0.5 ± 1.7)	0.53 ± 0.09 (0.49 ± 0.07)
1998	16.5 ± 2.0 (15.3 ± 1.6)	6.8 ± 1.8 (7.0 ± 1.2)	-0.6 ± 2.6 (-0.3 ± 1.7)	0.52 ± 0.08 (0.52 ± 0.07)
2000	12.5 ± 2.0 (14.6 ± 1.5)	6.3 ± 2.0 (6.6 ± 1.0)	-1.5 ± 3.6 (-0.4 ± 1.7)	0.52 ± 0.08 (0.55 ± 0.07)
Mean	16.2 ± 0.9 (16.1 ± 0.7)	7.1 ± 0.9 (7.0 ± 0.5)	-0.1 ± 1.5 (0.0 ± 0.8)	0.53 ± 0.04 (0.52 ± 0.03)

In the inverse model context we can answer this by holding the overturning to a fixed value and examining the solution for inconsistencies. Thus, our first set of experiments addresses this fundamental question in a manner uniquely available to our inverse model formalism. We ran a set of experimental inversions with the net overturning strength at 48°N constrained to be 16.1 ± 0.1 Sv (the mean of the unconstrained inversions discussed below). Although solutions were found, changes in individual layer transports across 48°N fall significantly outside the time-mean value for many layers and repeats. Inversions forced to a time-invariant overturning structure—implemented by adding a constraint that all individual layer transports across 48°N vary by no more than 1% from their time-mean value—fail to satisfy the prior demands. We conclude that the main information provided by these experimental inversions is to help determine the significance of temporal variations in the results. Differences in internal baroclinic exchange are present, and we proceed to examine solutions for these differences without imposing constraints on the net overturning strength or the individual layer transports across 48°N.

Transports across 48°N in the individual inverse model solutions, one for each of the five repeat lines, are given in Table 3.

Absolute velocity fields from these inversions are shown in Fig. 7. The velocity fields demonstrate the barotropic nature of the NAC in these solutions and the generally weaker adjustments introduced in the interior, because the thermal wind reference level (at the top of the LSW layer) remains very close to zero velocity east of ~40°W.

Vertically accumulated layer transport (i.e., the overturning streamfunction) is displayed for the inverse model solutions in Fig. 8. As was the case with the thermal wind calculations, the overturning is consistently larger than the air–sea transformation maxima for the subpolar North Atlantic. The discrepancy is accounted for by additional overturning across the Greenland–Scotland section, ultimately due to air–sea

transformation in the Nordic seas (not included explicitly in the model). Among the sections, differences in the overturning across 48°N are found essentially in the deeper, southward-flowing layers.

In Fig. 8 (right) we also illustrate the vertically integrated horizontal structure of each of the solutions. Large southward flow near 50 Sv in 1997 and 2000 is shown inshore of the NAC. Similar values were found by Meinen et al. (2000) on a limited transect across the NAC in 1993, but we have no direct evidence supporting large values during the 1997 section. The large value for the 2000 section is consistent with the 1999–2001 DWBC transport time series of Schott et al. (2004, their Fig. 13a). In the NAC, vertically integrated transports of 90–150 Sv are found with an immediate recirculation of 50–80 Sv, the largest values occurring in 2000 and the smallest occurring in 1998. Farther offshore the flow can be either generally southward over the Mid-Atlantic Ridge (MAR) western flank (1996; the MAR crests at 28°W at this latitude) or generally northward over the same region (1997), with similar reversals over the eastern flank. As before, the differences are barely significant. Northward and southward flows above the flanks are observed as barotropic wind-driven variability in numerical models (Gulev et al. 2003; Eden and Willebrand 2001), possibly consistent with the horizontal structure observed in Fig. 8; however, uncertainties in both observations and models make detailed comparisons of little apparent value.

To illustrate the estimated changes in transport in relation to mixing assumptions, the total overturning amplitude and results for two deep-water masses are displayed for two different models (Fig. 9). The first model (Fig. 9, left) allows diapycnal mixing to vary for each year. The second model (Fig. 9, right) requires diapycnal mixing to be constant (the ensemble mean value from the variable-mixing inversions) for all years. For layers that do not outcrop, variations in export balance storage in the fixed-mixing inversions; in the variable-mixing inversions, this can balance changes in export for nonoutcropping layers.

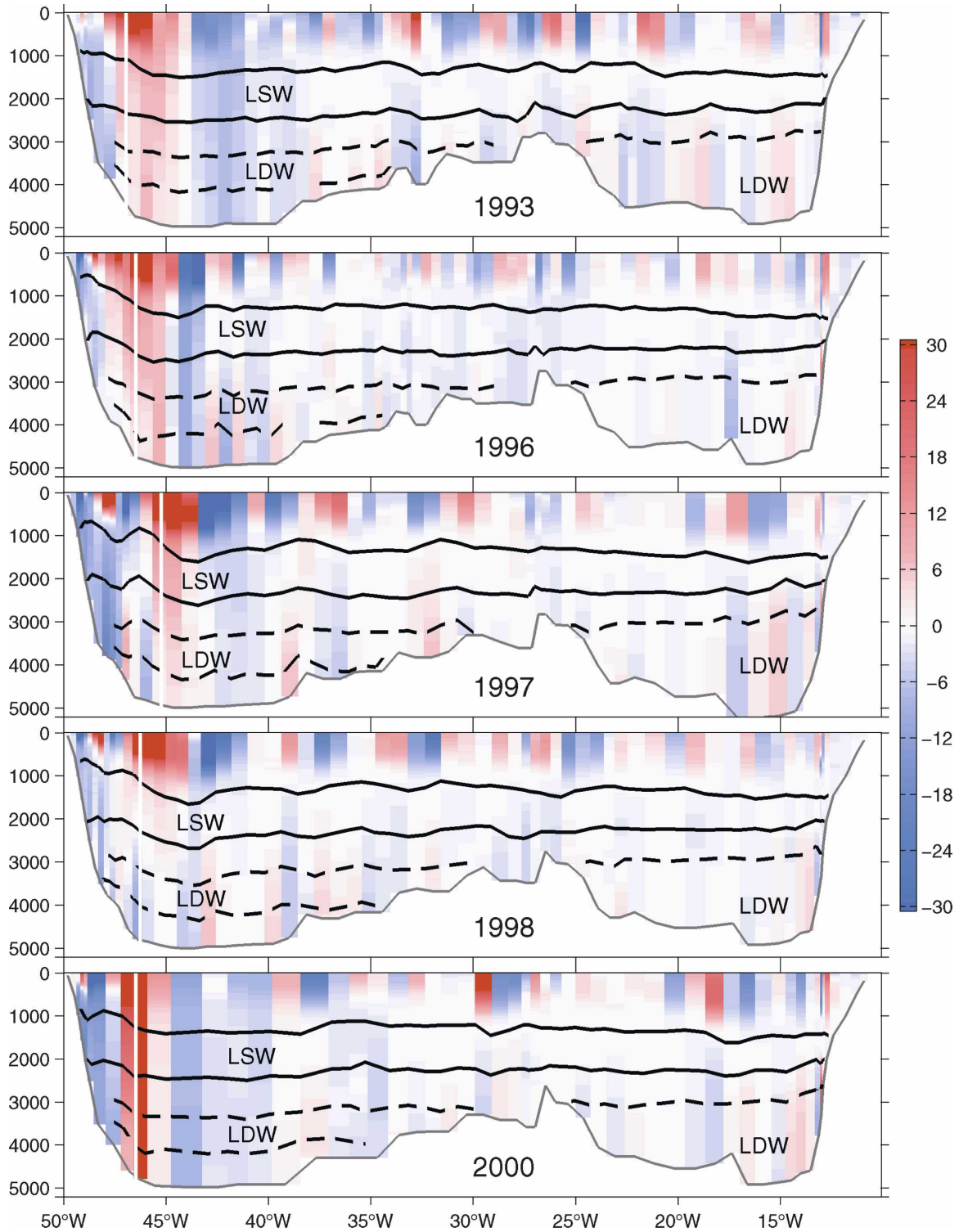


FIG. 7. Absolute velocity at 48°N (cm s^{-1}) from the inverse model solutions (positive northward). Neutral-density layers indicated as in Fig. 3.

Changes in overturning strength (Fig. 9, top) are, with one exception, consistent within error bars with the preinversion calculations (Fig. 4; nonzero reference velocity values). The exception is the 2000 repeat, for

which the inversion decreases the northward transport and interior recirculation in the western region as well as reduces the southward transport of the DWBC. This adjustment diminishes the deep overturning cell noted

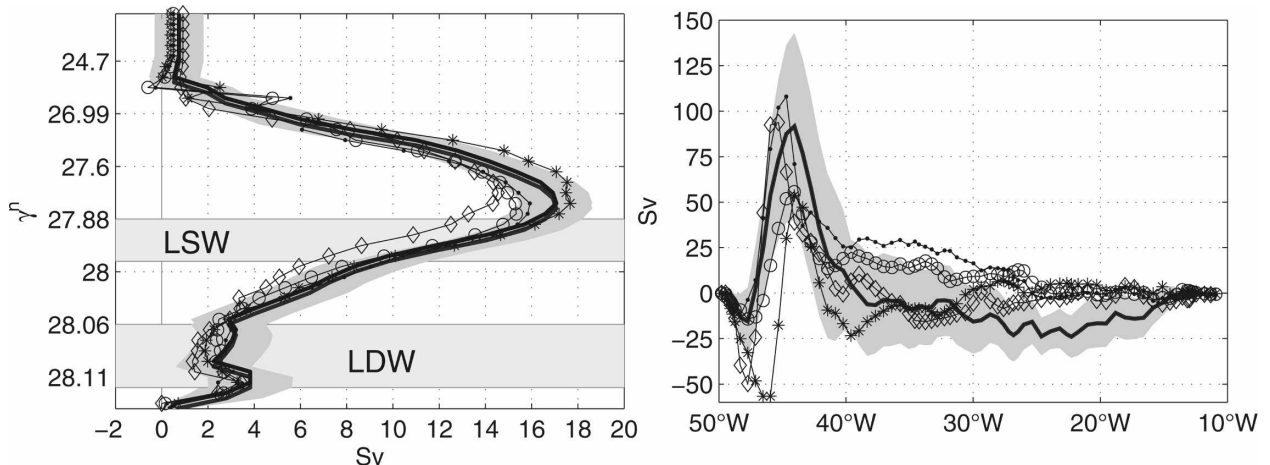


FIG. 8. (left) Cumulative bottom-to-top-layer transport (overturning streamfunction; positive southward) across 48°N in the inverse box model solutions. Heavy line with shaded error bar is the 1993 repeat; other repeats (error bars not shown, but similar to 1993) are 1996 (dots), 1997 (asterisks), 1998 (circles), and 2000 (diamonds). Horizontal lines indicate the density range of LSW and LDW. The vertical axis is the model layer, which is not linearly distributed in neutral-density space but represents approximately equal volumes of the world's oceans. (right) Cumulative west-east transport of all layers (from top to bottom), showing the vertically integrated structure of the NAC, the Mann Eddy recirculation, and the flow farther east.

in section 3a and increases the net overturning from 9.3 to 14.6 ± 1.5 Sv (time-invariant inversion).

Variations in heat transport across 48°N calculated by the inverse model are small compared to variations in net subpolar heat loss (Fig. 9). On average, 0.53 ± 0.1 PW is carried northward across 48°N by the ocean, and 0.28 PW is lost to the atmosphere in the subpolar North Atlantic. The remaining 0.25 PW is carried by the ocean farther north, out of the model domain and into the Nordic seas. In the inverse model solutions, variations in subpolar oceanic heat loss are associated with variations in heat transport across the Greenland–Scotland section (e.g., the Norwegian Atlantic Current) and in heat storage.

The model adjusts net heat and freshwater fluxes from the prior choices. For the inversions of the 1993 and 1996 sections, the solution is consistent with the larger heat loss of the NOC product, but it rejects (i.e., it is larger within the formal error bar) the relatively weak loss from outcropping layers in the density range of $26 < \gamma^\sigma < 27.2$ given by the NCEP–NCAR product. For the 1997 section, the model-adjusted heat flux is consistent with NCEP–NCAR fluxes and significantly weaker than NOC in the range of $25.8 < \gamma^\sigma < 27$. Adjusted freshwater fluxes remain consistent with both products.

In the inverse model solutions, much of the Labrador Sea Water exported across 48°N is generated within the subpolar North Atlantic by diapycnal mixing rather than directly by air–sea transformation. This mixing is associated with a downward diapycnal advection of about 6 Sv across the upper LSW interface $\gamma^\sigma = 27.88$,

with a smaller conversion of LSW to denser layers (Fig. 10). For the inversions with time-invariant mixing, section-to-section differences in transport across 48°N are generated by differences in the air–sea formation rate of LSW. In Lower Deep Water layers, mixing supplies about 3 Sv from bottom water and removes a similar amount across the upper interface (Fig. 10). Air–sea formation and storage changes roughly compensate each other from section to section, and the apparent trend (Fig. 9) would be because of a lower export, that is, a reduced southward geostrophic transport of Lower Deep Water.

5. Discussion

Inverse box model solutions were sought that consistently balance lateral transport in isopycnal layers, diapycnal fluxes, and air–sea formation rates. Although the diapycnal fluxes were allowed to vary in one set of runs along with the horizontal flow and air–sea fluxes, none of the solutions showed a significant change in the diapycnal fluxes, and no trend was seen in the variations of mixing from one solution to the next.

The inverse model solutions suggest that mixing plays a major role in the maintenance of the large-scale Labrador Sea Water layer. The balance between heat loss to the atmosphere and lateral eddy fluxes of heat and salt may govern the variations of wintertime convective depth in the Labrador Sea (Lazier et al. 2002). Lilly et al. (2003) report that about one-third of the missing lateral heat and salt fluxes appears to be accounted for by eddies. Our results apply to a more

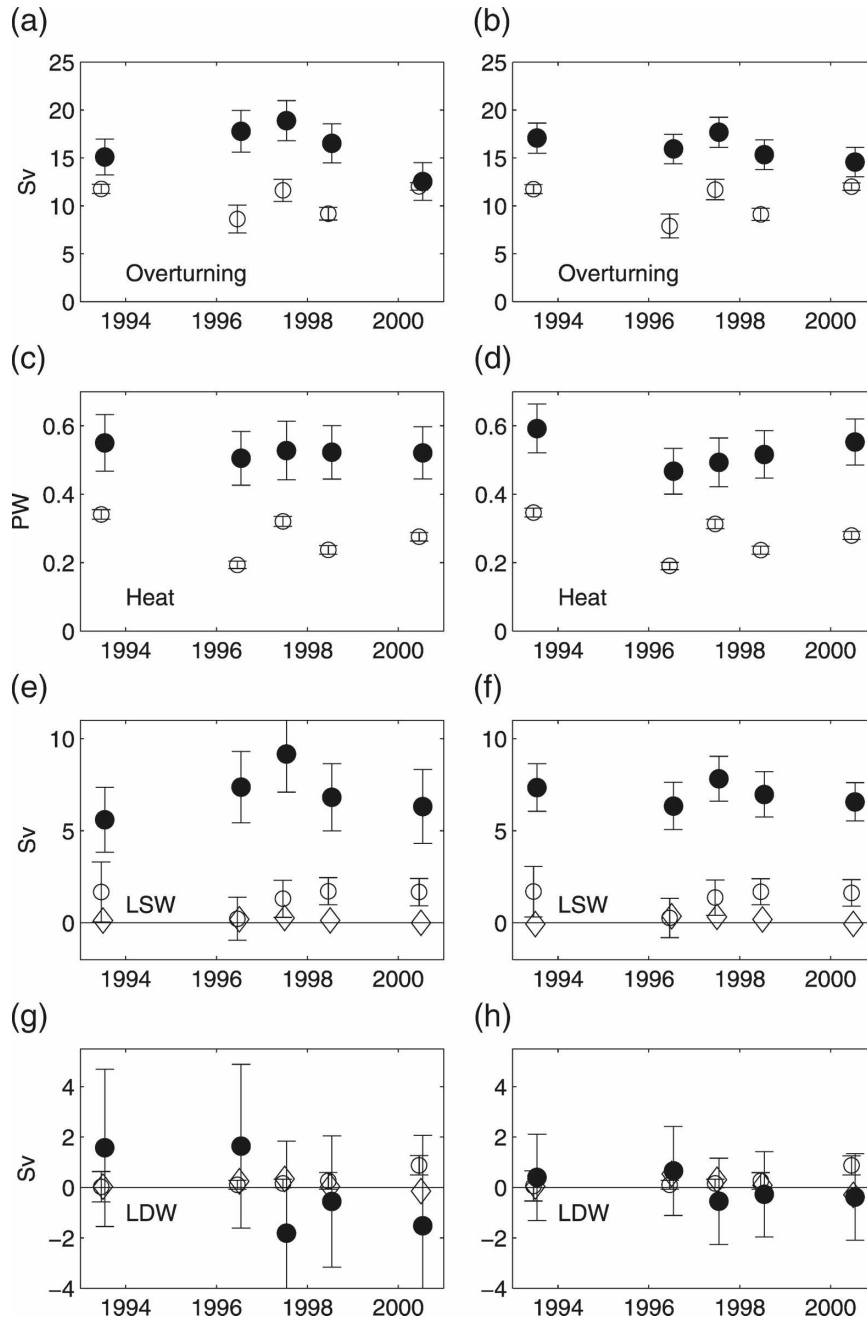


FIG. 9. Transports from the inverse model solutions. (left) Time-varying mixing inversions; (right) inversions with time-invariant mixing. (a), (b) Overturning strength (black bullets) across 48°N and net air-sea formation of dense water (open circles) in the subpolar North Atlantic. (c), (d) Northward transport of heat across 48°N (black bullets; Ekman component included) and subpolar heat loss to the atmosphere (open circles). (e)–(h) Southward (positive) export (black bullets), air-sea formation (circles), and residual/storage (diamonds) of (e), (f) LSW and (g), (h) LDW.

broadly defined range of densities than the convective patch in the central Labrador Sea but support the concept that mixing is an important component of the balance, at least in that particular broader density range.

The detailed diapycnal balance is consistent with a mass transfer from lighter densities to the Labrador Sea Water layer; diapycnal transfer to this layer from a higher density is 0–2 Sv (Fig. 10).

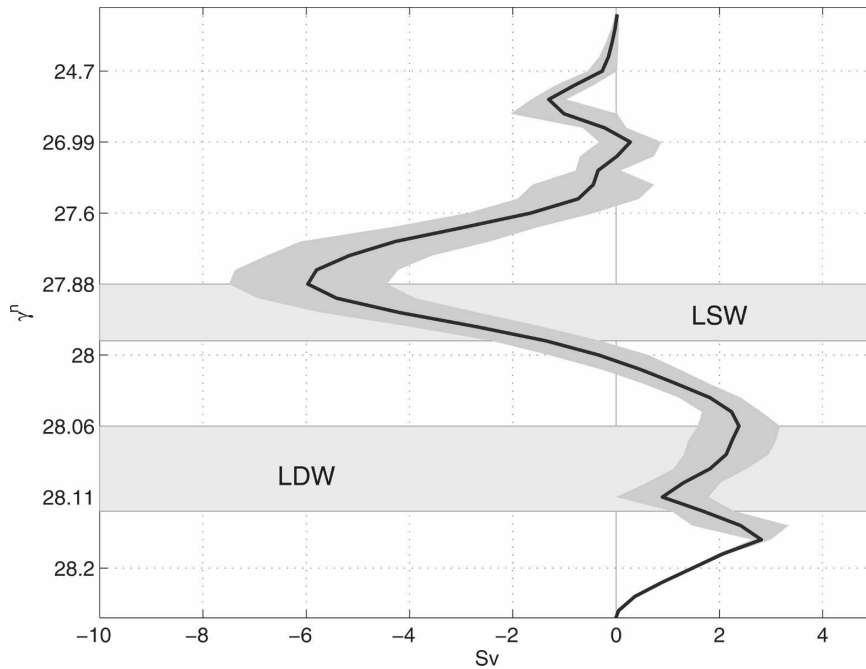


FIG. 10. Time-invariant diapycnal volume flux across the layer interfaces, driven by mixing in the subpolar North Atlantic and diagnosed from the inverse model solutions. Positive is upward (dense-to-light conversion). Convergence (as seen in the LSW layers) corresponds to mixing-driven formation. The vertical axis is model layer, which is not linearly distributed in neutral-density space but represents approximately equal volumes of the world's oceans.

The inverse model solutions show less variability in overturning than do previous studies (Koltermann et al. 1999; Lorbacher and Koltermann 2000; Marsh 2000). Stammer et al. (2003) did not display overturning, but their deep transport time series suggests a variability of 2–3 Sv at seasonal scales. We find low-amplitude changes similar to seasonally or annually averaged numerical model simulations of overturning (e.g., Beisemann et al. 2002), partly reflecting the constraints and choices made in the construction of the model.

Lower Deep Water transports with a middepth reference level showed very large changes, which were tempered by the inverse model to a weak, insignificant downward trend. The (fixed mixing) inversions have a LDW export trend of -1.4 ± 3.0 Sv decade⁻¹. Whether this is part of a longer period reversal or a partial shutdown is unclear from the observations used in this study. With fewer sections, but covering a wider time span, Bryden et al. (2005) inferred a roughly 50% net reduction in LDW transport at 25°N, also corresponding to 1–2 Sv decade⁻¹. Their definition of the LDW was somewhat broader and deeper (denser) than ours, but it seems doubtful that their estimate of a trend at 25°N is any more significant than ours.

The uncertainties are large in our solutions, and very little can be said about important details of the merid-

ional flow. The initial-state (preinversion) velocities on the thermal wind reference level are meant to reflect time-mean conditions in the presence of a meandering North Atlantic Current and Mann Eddy. They do not reflect temporal variations in the net transports of this current system; the inversion may or may not improve this for the repeat lines. We can only claim that the nonzero reference velocities constitute a reasonable starting point in the absence of direct flow observations over time. It may not be surprising that in the end we arrive at an estimate of net overturning that deviates little from an average state. On the other hand, the magnitude of this average state, the variations, and the expected error are all results of the ensemble of constraints, variance estimates, and forcing used in the model. They provide quantitative bounds, or what might be considered reasonable limits, on overturning and heat transport and could be of use in comparison to numerical simulations.

At the very least, direct quantitative transport information that resolves the narrow spatial structure in the western boundary current system, and probably flow over the midocean ridge and eastern boundary as well, is needed, but it is difficult to obtain. Large-scale variability might also be addressed by investigations with numerical models and data assimilation, but the results

from such models depend on the way in which mixing, eddies, and overflows are parameterized, and thus questions will remain until such parameterizations improve.

Acknowledgments. Support for KS and RL from NSF Grant OCE-9906657 for WOCE data analysis is appreciated. Additional support for RL was provided by the NOAA/Office of Climate Observations and the Atlantic Oceanographic and Meteorological Laboratory. The German WOCE and CLIVAR programs supported observations on 48°. The chief scientist on WOCE AR19 (A2) was A. Sy (Gauss, 12 June–31 July 1993). The CLIPPER numerical model output was provided by A.-M. Treguier, with support from the CNRS and IDRIS. The NCEP–NCAR reanalysis data are provided by the NOAA/CIRES Climate Diagnostics Center, Boulder. The NAO index is an updated version of the Hurrell Lisbon–Stykkisholmur December–March index, by T. Mitchell (JISAO). The Southampton reanalysis of the COADS air–sea fluxes was provided by J. Grist and S. Josey. C. Meinen generously provided data from the western boundary current array and offered invaluable advice for incorporating this information into the inverse model. Comments from F. Schott and M. Baringer helped to improve the original manuscript. The findings and conclusions in this report are those of the authors and do not necessarily represent the views of the funding agencies.

APPENDIX

Details of the Inverse Model

Gauss–Markov inversion requires a specified acceptable tolerance level for conservation of various properties (imposed as integral constraints), referred to as the model errors, and estimates of magnitude of the unknowns that specify an allowed range for their adjustment. All inversions can include additional constraints on transports in individual layers or blocks of layers, which are applied over a net section or individual station pairs of a section.

a. Integral constraints

In the inversions presented here, net mass in the subpolar box was conserved to 0 ± 1 Sv. Riverine input was included from the Global Runoff Data Center database of Grabs et al. (1996); this amounted to 0.26 Sv added to the lightest layer in the subpolar box. The volume of each layer with a density of $\gamma'' > 25.3$ (layers 7–45) was required to be conserved to ± 0.5 Sv. The lightest layer, $\gamma'' < 21.8$, was conserved to ± 3 Sv; layers 2–6 were

conserved to values linearly interpolated (by layer number) between 3 and 0.5 Sv. The reduction in volume conservation in the upper layers follows the work of Ganachaud (2003) and is intended to accommodate seasonal variations in the upper-baroclinic structure of the section when one is attempting to resolve annual-mean transports. Net and layer budgets of the salt anomaly and potential temperature were constrained to the mean value (averaged over the subpolar Atlantic for net conservation and the neutral-density layer for layer conservation) of the property, plus twice the standard deviation of the property (Ganachaud 2003), multiplied by the corresponding volume model error. This mean and standard deviation were calculated directly from the bounding sections of the subpolar box.

Salt anomaly with respect to 35 psu was conserved, rather than conserving total salt in the layers. This serves to separate mass and salt conservation (cf. Ganachaud 1999). One could in principle conserve salt anomaly with respect to section- and layer-mean salinities, rather than with respect to 35 psu. This could gain additional separation between mass and salt conservation equations. We did not do this here, because we judged that the slight additional gain would be offset by the bookkeeping effort and potential introduction of errors associated with diapycnal advection of salt from one layer to another.

b. Section-specific constraints

The Bering Strait throughflow of mass and salt enters the North Atlantic primarily via the Canadian Archipelago (Wijffels et al. 1992). To include this in our inversion at appropriate density layers, we constructed a simulated hydrographic section at 79°N, 70.5°–72.5°W from three grid points in the Gouretski and Jancke (1998) hydrographic climatology. Volume transport for this “section” was constrained to be 0.9 ± 0.2 Sv southward, representing the Bering Strait throughflow and Arctic ice melt and riverine input (Coachman and Aagaard 1988). Volume transport across the Greenland–Scotland Ridge sections was constrained to be 0 ± 0.3 Sv. Salt transport across all northern bounding sections, including the virtual Canadian Archipelago section, was constrained to the Bering Strait throughflow of $(26.7 \pm 19) \times 10^6$ kg s⁻¹ southward (Wijffels et al. 1992).

For AR18 (Denmark Strait), thermal wind was calculated relative to a bottom reference level. Constraints were imposed to reproduce a more realistic flow structure (LS03): a Denmark Strait overflow of 2.0 ± 0.2 Sv southward for $\gamma'' > 28.14$, and 0.9 ± 0.1 Sv southward for $28.01 < \gamma'' < 28.14$ (Girton et al. 2001); polar water flow in the East Greenland Current of 1.6 ± 0.5 Sv

southward in the westernmost 15 station pairs for $\gamma^n < 27.6$ (Malmberg et al. 1972; Mauritzen 1996); and an Irminger Current branch of 0.9 ± 0.4 Sv northward in the easternmost five station pairs for $\gamma^n < 27.6$ (Mauritzen 1996).

For the composite Iceland–Scotland Ridge sections, a thermal wind reference level of $\gamma^n = 27.88$ was chosen, separating northward-flowing Norwegian Atlantic water from southward-flowing overflow. Constraints were a Faroe Bank Channel overflow of 1.4 ± 0.2 Sv southward for $\gamma^n > 28.14$ (Saunders 1990; Mauritzen 1996; Østerhus et al. 1999; Price et al. 2001), an overflow across the Iceland–Faroe Rise of 0.85 ± 0.30 Sv southward in the westernmost 14 pairs for $\gamma^n > 27.88$ (Saunders 1990; Mauritzen 1996), a flow of Atlantic water across the Iceland–Faroe Rise of 4.0 ± 0.4 Sv northward in the westernmost 14 pairs for $\gamma^n < 27.88$ (Hansen et al. 1999), and a Norwegian Atlantic Current between the Faroe Islands and Scotland of 3.0 ± 0.4 Sv northward in the easternmost 18 pairs for $\gamma^n < 27.88$ (Gould et al. 1985; Mauritzen 1996; Hansen et al. 1999).

c. Adjustments to unknowns

Allowed adjustments to the unknown reference velocities, interior mixing terms, and adjustments to the air–sea heat and freshwater fluxes were contained in a prior variance matrix (Wunsch 1996). In the absence of knowledge regarding the full covariance structure of this matrix, we assumed it to be diagonal.

Adjustments to reference velocities were required to be in a range of $\pm v_{\text{ref}|_{\text{ap}}}$. For all northern sections, this value was assumed to be 10 cm s^{-1} in all pairs, to represent potentially strong barotropic adjustments.

One significant change was made from LS03: in that study, the $v_{\text{ref}|_{\text{ap}}}$ was chosen to be $\pm 2 \text{ cm s}^{-1}$ for all AR19 pairs east of the western boundary (100-km width) and $\pm 30 \text{ cm s}^{-1}$ for the western boundary pairs. These choices were similar to other inverse studies (Macdonald 1998; Ganachaud 1999). The large western boundary value was intended to permit (or at least not to preclude) a realistic NAC strength in the inverse solution. With the more careful consideration of the NAC and Mann Eddy structure here, we decided to allow adjustments of 10 cm s^{-1} magnitude to all pairs west of 40°W , linearly decreasing from 10 to 5 cm s^{-1} at 35°W , and linearly decreasing to 2 cm s^{-1} at 10°W . The western boundary value is supported by the IES dataset, which shows standard deviations near 10 cm s^{-1} at the reference level. Smaller values to the east of 40°W , and much smaller values in the eastern basin, are supported by distributions of eddy kinetic energy from altimetry and surface drifters (cf. Fratantoni 2001).

Prior variances for the adjustments to the air–sea heat and freshwater fluxes F^* were taken as the range of the NOC COADS– and NCEP-derived calculations. In other words, where the climatologies produce transformation curves that agreed to within 0.1 Sv on a given density layer, the resulting flux could only be adjusted to ± 0.1 Sv from the prior (mean from the three products) value; a large discrepancy allowed the model to adjust more dramatically.

The interior mixing of density, salt, and heat $\partial_\rho D$ can be written as effective diffusivities (cf. LS03), which include both explicit diffusion and eddy mixing in a Reynolds decomposition sense. While observations of these processes at particular locations have been collected, little is known in regards to their large-scale integrated values for a given density layer. In this study, the allowed magnitude of the property-dependent mixing terms was calculated from the preinversion convergence or divergence of the property, with a uniform 2-Sv additional “slop” added to allow adjustments in layers with very small preinversion imbalances. Allowed magnitudes for the diapycnal transfer terms representing heat and salt anomaly diffusion were calculated similarly, with the slop set by 2 Sv times the layer-averaged mean plus twice the standard deviation.

REFERENCES

- Bacon, S., 1997: Circulation and fluxes in the North Atlantic between Greenland and Ireland. *J. Phys. Oceanogr.*, **27**, 1420–1435.
- Beismann, J. O., C. W. Boening, and D. Stammer, 2002: Interannual to decadal variability of the meridional overturning circulation of the Atlantic: A comparison of the response to atmospheric fluctuations in three ocean models. *CLIVAR Exchanges*, No. 25, International CLIVAR Project Office, Southampton, United Kingdom, 34–46.
- Bersch, M., 2002: North Atlantic Oscillation–induced changes of the upper layer circulation in the northern North Atlantic Ocean. *J. Geophys. Res.*, **107**, 3156, doi:10.1029/2001JC000901.
- Bryan, K., 1962: Measurements of meridional heat transport by ocean currents. *J. Geophys. Res.*, **67**, 3403–3414.
- Bryden, H. L., and S. Imawaki, 2001: Ocean heat transport. *Ocean Circulation and Climate*, G. Siedler, J. Church, and J. Gould, Eds., International Geophysical Series, Vol. 77, Academic Press, 455–474.
- , H. R. Longworth, and S. A. Cunningham, 2005: Slowing of the Atlantic meridional overturning circulation at 25°N . *Nature*, **438**, 655–657.
- Coachman, L., and K. Aagaard, 1988: Transports through Bering Strait: Annual and interannual variability. *J. Geophys. Res.*, **93**, 15 535–15 539.
- Dickson, B., I. Yashayaev, J. Meincke, B. Turrell, S. Dye, and J. Holfort, 2002: Rapid freshening of the deep North Atlantic Ocean over the past four decades. *Nature*, **416**, 832–837.
- Eden, C., and T. Jung, 2001: North Atlantic interdecadal variability: Oceanic response to the North Atlantic Oscillation (1865–1997). *J. Climate*, **14**, 676–691.

- , and J. Willebrand, 2001: Mechanism of interannual to decadal variability of the North Atlantic circulation. *J. Climate*, **14**, 2266–2280.
- Fratantoni, D. M., 2001: North Atlantic surface circulation during the 1990's observed with satellite-tracked drifters. *J. Geophys. Res.*, **106**, 22 067–22 093.
- Ganachaud, A., 1999: Large scale oceanic circulation and fluxes of freshwater, heat, nutrients, and oxygen. Ph.D. thesis, Massachusetts Institute of Technology, 249 pp.
- , 2003: Error budget of inverse box models: The North Atlantic. *J. Atmos. Oceanic Technol.*, **20**, 1641–1655.
- Girton, J. B., T. B. Sanford, and R. H. Käse, 2001: Synoptic sections of the Denmark Strait overflow. *Geophys. Res. Lett.*, **28**, 1619–1622.
- Gould, W. J., L. Loynes, and J. Backhaus, 1985: Seasonality in slope current transports NW of Shetland. ICES Hydrography Committee CM C7, International Council for the Exploration of the Sea, 13 pp.
- Gouretski, V., and K. Jancke, 1998: A new World Ocean climatology: Optimal interpolation of historical and WOCE hydrographic data on neutral surfaces. WOCE Rep. 162/98, WOCE Special Analysis Center, Max Planck Institute, Hamburg, Germany, 40 pp.
- Grabs, W., T. de Couet, and J. Pauler, 1996: Freshwater fluxes from continents into the world oceans based on data of the Global Runoff Data Base. Tech. Rep. 10, Global Runoff Data Centre, Koblenz, Germany, 49 pp.
- Grist, J. P., and S. A. Josey, 2003: Inverse analysis adjustment of the SOC air–sea flux climatology using ocean heat transport constraints. *J. Climate*, **16**, 3274–3295.
- Gulev, S. K., B. Barnier, H. Knochel, J.-M. Molines, and M. Côtet, 2003: Water mass transformation in the North Atlantic and its impact on the meridional circulation: Insights from an ocean model forced by NCEP–NCAR reanalysis surface fluxes. *J. Climate*, **16**, 3085–3110.
- Häkkinen, S., 1999: Variability of the simulated meridional heat transport in the North Atlantic for the period 1951–1993. *J. Geophys. Res.*, **104**, 10 991–11 007.
- Hall, M. M., and H. L. Bryden, 1982: Direct estimates and mechanisms of ocean heat transport. *Deep-Sea Res.*, **29**, 339–359.
- Hansen, B., K. M. H. Larsen, S. Østerhus, B. Turrell, and S. Jónsson, 1999: The Atlantic Water Inflow to the Nordic Seas. *International WOCE Newsletter*, No. 35, WOCE International Project Office, Southampton, United Kingdom, 33–35.
- Hurrell, J. W., 1995: Decadal trends in the North Atlantic Oscillation: Regional temperatures and precipitation. *Science*, **269**, 676–679.
- Jackett, D. R., and T. J. McDougall, 1997: A neutral density variable for the world's oceans. *J. Phys. Oceanogr.*, **27**, 237–263.
- Josey, S. A., E. C. Kent, and P. K. Taylor, 1998: *The Southampton Oceanography Centre (SOC) Ocean–Atmosphere Heat, Momentum, and Freshwater Flux Atlas*. SOC Rep. 6, Southampton Oceanography Centre, 30 pp.
- Kalnay, E., and Coauthors, 1996: The NCEP/NCAR 40-Year Reanalysis Project. *Bull. Amer. Meteor. Soc.*, **77**, 437–471.
- Koltermann, K. P., A. Sokov, V. Tereschenkov, S. Dobroliubov, K. Lorbacher, and A. Sy, 1999: Decadal changes in the thermohaline circulation of the North Atlantic. *Deep-Sea Res. II*, **46**, 109–138.
- Large, W. G., and A. J. Nurser, 2001: Ocean surface water mass transformation. *Ocean Circulation and Climate*, G. Siedler, J. Church, and J. Gould, Eds., International Geophysical Series, Vol. 77, Academic Press, 317–336.
- Latif, M., C. Böning, J. Willebrand, A. Biastoch, J. Dengg, N. Keenlyside, U. Schreckendiek, and G. Madec, 2006: Is the thermohaline circulation changing? *J. Climate*, **19**, 4631–4637.
- Lazier, J., R. Hendry, A. Clarke, I. Yashayaev, and P. Rhines, 2002: Convection and restratification in the Labrador Sea, 1990–2000. *Deep-Sea Res. I*, **49**, 1819–1835.
- Levitus, S., and T. P. Boyer, 1994: *Temperature*. Vol. 4, *World Ocean Atlas 1994*, NOAA Atlas NESDIS 4, 117 pp.
- , R. Burgett, and T. P. Boyer, 1994: *Salinity*. Vol. 3, *World Ocean Atlas 1994*, NOAA Atlas NESDIS 3, 99 pp.
- Lilly, J. M., P. B. Rhines, F. Schott, K. Lavender, J. Lazier, U. Send, and E. D'Asaro, 2003: Observations of the Labrador Sea eddy field. *Prog. Oceanogr.*, **59**, 75–176.
- Lorbacher, K., and P. Koltermann, 2000: Subinertial variability of transport estimates across 48°N in the North Atlantic. *International WOCE Newsletter*, No. 40, WOCE International Project Office, Southampton, United Kingdom, 3–5.
- Lumpkin, R., and K. Speer, 2003: Large-scale vertical and horizontal circulation in the North Atlantic Ocean. *J. Phys. Oceanogr.*, **33**, 1902–1920.
- Macdonald, A. M., 1998: The global ocean circulation: A hydrographic estimate and regional analysis. *Prog. Oceanogr.*, **41**, 281–382.
- Macrandar, A., U. Send, H. Valdimarsson, S. Jónsson, and R. H. Käse, 2005: Interannual changes in the overflow from the Nordic Seas into the Atlantic Ocean through Denmark Strait. *Geophys. Res. Lett.*, **32**, L06606, doi:10.1029/2004GL021463.
- Malmberg, S. A., H. G. Gade, and H. E. Sweers, 1972: Current velocities and volume transports in the East Greenland Current off Cape Nordenskjöld in August–September 1965. *Sea Ice: Proceedings of an International Conference*, T. Karlsson, Ed., National Research Council of Iceland, 130–139.
- Mann, C. R., 1967: The termination of the Gulf Stream and the beginning of the North Atlantic Current. *Deep-Sea Res.*, **14**, 337–359.
- Marsh, R., 2000: Recent variability of the North Atlantic thermohaline circulation inferred from surface heat and freshwater fluxes. *J. Climate*, **13**, 3239–3260.
- Mauritzen, C., 1996: Production of dense overflow waters feeding the North Atlantic across the Greenland–Scotland Ridge. *Deep-Sea Res. I*, **43**, 769–835.
- , and S. Häkkinen, 1999: On the relationship between dense water formation and the “Meridional Overturning Cell” in the North Atlantic Ocean. *Deep-Sea Res. I*, **46**, 877–894.
- Meinen, C. S., 2001: Structure of the North Atlantic Current in stream-coordinates and the circulation in the Newfoundland basin. *Deep-Sea Res. I*, **48**, 1553–1580.
- , and D. R. Watts, 2000: Vertical structure and transport on a transect across the North Atlantic Current near 42°N: Time series and mean. *J. Geophys. Res.*, **105**, 21 869–21 891.
- , —, and R. A. Clarke, 2000: Absolutely referenced geostrophic velocity and transport on a section across the North Atlantic Current. *Deep-Sea Res. I*, **47**, 309–322.
- Niiler, P. P., N. A. Maximenko, and J. C. McWilliams, 2003: Dynamically balanced absolute sea level of the global ocean derived from near-surface velocity observations. *Geophys. Res. Lett.*, **30**, 2164, doi:10.1029/2003GL018628.
- Østerhus, S., B. Hansen, R. Kristiansen, and P. Lundberg, 1999: The overflow through the Faroe Bank Channel. *International WOCE Newsletter*, No. 35, WOCE International Project Office, Southampton, United Kingdom, 35–37.
- Price, J., T. Sanford, C. Mauritzen, and M. Prater, 2001: A report of XCP and CTD data taken during June 2001 RRS Discov-

- ery cruise 247B: A process study of the Faroe Bank Channel Overflow. Woods Hole Oceanographic Institution Res. Rep., 60 pp. [Available online at <http://www.whoi.edu/science/PO/people/jprice/oflow/FBC.pdf>.]
- Reiniger, R. F., and R. A. Clarke, 1975: Circulation pattern in the Newfoundland Ridge area, 1972. *Proc. Symp. on Environmental Conditions in the Newfoundland Grand Bank Area in 1972 and Their Effect on Fishery Trends* (Special Publication 10), International Commission for Northwest Atlantic Fisheries, 57–67.
- Robbins, P. E., and J. M. Toole, 1997: The dissolved silica budget as a constraint on the meridional overturning circulation of the Indian Ocean. *Deep-Sea Res. I*, **44**, 879–906.
- Saunders, P. M., 1990: Cold outflow from the Faroe Bank Channel. *J. Phys. Oceanogr.*, **20**, 29–43.
- Schott, F. A., R. Zantopp, L. Stramma, M. Dengler, J. Fischer, and M. Wibaux, 2004: Circulation and deep-water export at the western exit of the subpolar North Atlantic. *J. Phys. Oceanogr.*, **34**, 817–843.
- , J. Fischer, M. Dengler, and R. Zantopp, 2006: Variability of the Deep Western Boundary Current east of the Grand Banks. *Geophys. Res. Lett.*, **33**, L21S07, doi:10.1029/2006GL026563.
- Shaffrey, L., and R. Sutton, 2004: The interannual variability of energy transports within and over the Atlantic Ocean in a coupled climate model. *J. Climate*, **17**, 1433–1448.
- Speer, K. G., 1997: A note on average cross-isopycnal mixing in the North Atlantic Ocean. *Deep-Sea Res. I*, **44**, 1981–1990.
- Stammer, D., and Coauthors, 2003: Volume, heat, and freshwater transports of the global ocean circulation 1993–2000, estimated from a general circulation model constrained by World Ocean Circulation Experiment (WOCE) data. *J. Geophys. Res.*, **108**, 3007, doi:10.1029/2001JC001115.
- Stramma, L., D. Kieke, M. Rhein, F. Schott, I. Yashayaev, and K. P. Koltermann, 2004: Deep water changes at the western boundary of the subpolar North Atlantic during 1996 to 2001. *Deep-Sea Res. I*, **51**, 1033–1056.
- Treguier, A.-M., O. Boebel, B. Barnier, and G. Madec, 2003: Agulhas eddy fluxes in a 1/6° Atlantic model. *Deep-Sea Res. II*, **50**, 251–280.
- Walin, G., 1982: On the relation between sea-surface heat flow and thermal circulation in the ocean. *Tellus*, **34**, 187–195.
- Wijffels, S. E., R. W. Schmitt, H. L. Bryden, and A. Stigebrandt, 1992: Transport of freshwater by the oceans. *J. Phys. Oceanogr.*, **22**, 155–162.
- Wunsch, C., 1996: *The Ocean Circulation Inverse Problem*. Cambridge University Press, 442 pp.